Inorganic Chemistry

Article

pubs.acs.org/IC

Redox Chemistry of Nickel(II) Complexes Supported by a Series of Noninnocent β-Diketiminate Ligands

June Takaichi,[†] Yuma Morimoto,[†] Kei Ohkubo,[†] Chizu Shimokawa,[‡] Takayuki Hojo,[§] Seiji Mori,*[,§] Haruyasu Asahara,[∥] Hideki Sugimoto,[†] Nobutaka Fujieda,[†] Nagatoshi Nishiwaki,[∥] Shunichi Fukuzumi,[†] and Shinobu Itoh*[,†]

[†]Department of Material and Life Science, Division of Advanced Science and Biotechnology, Graduate School of Engineering, Osaka University, 2-1 Yamadaoka, Suita, Osaka 565-0871, Japan

[‡]Department of Medical Biochemistry, Kurume University School of Medicine, Kurume, Fukuoka 830-0011, Japan

[§]Department of Chemistry, Faculty of Science, Ibaraki University, 2-1-1 Bunkyo, Mito, Ibaraki 310-8512, Japan

[∥]School of Environmental Science and Engineering, Kochi University of Technology, Tosayamada, Kami, Kochi, 782-8502, Japan

Supporting Information

ABSTRACT: Nickel complexes of a series of β-diketiminate ligands ($^{R}L^{-}$, deprotonated form of 2-substituted *N*-[3-(phenylamino)allylidene]aniline derivatives ^{R}LH, R = Me, H, Br, CN, and NO_2) have been synthesized and structurally characterized. One-electron oxidation of the neutral complexes $[Ni^{II}(^{R}L^{-})_2]$ by $AgSbF_6$ or $[Ru^{III}(bpy)_3](PF_6)_3$ (bpy = 2,2′-bipyridine) gave the corresponding metastable cationic complexes, which exhibit an EPR spectrum due to a doublet species ($S = 1/2$) and a characteristic absorption band in near IR region ascribable to a ligand-to-ligand intervalence charge-transfer (LLIVCT) transition. DFT calculations have indicated that the divalent oxidation state of nickel ion (Ni^{II}) is retained, whereas one of the β-diketiminate ligands is oxidized to give formally a mixed-valence complex, $[Ni^{II}(^{R}L^{-})(^{R}L^{\bullet})]^{+}$. Thus, the doublet spin state of the oxidized cationic complex can be explained by taking account of the antiferromagnetic interaction between the high-spin nickel(II) ion ($S = 1$) and the organic radical ($S = 1/2$) of supporting ligand. A single-crystal structure of one of the cationic complexes (R = H) has been successfully determined to show that both ligands in the cationic complex are structurally equivalent. On the basis of theoretical analysis of the LLIVCT band and DFT calculations as well as the crystal structure, the mixed-valence complexes have been assigned to Robin−Day class III species, where the radical spin is equally delocalized between the two ligands to give the cationic complex, which is best described as $[Ni^{II}(^{R}L^{0.5\bullet-})_2]^{+}$. One-electron reduction of the neutral complexes with decamethylcobaltocene gave the anionic complexes when the ligand has the electron-withdrawing substituent (R = CN, NO_2, Br). The generated anionic complexes exhibited EPR spectra due to a doublet species ($S = 1/2$) but showed no LLIVCT band in the near-IR region. Thus, the reduced complexes are best described as the d^9 nickel(I) complexes supported by two anionic β-diketiminate ligands, $[Ni^{I}(^{R}L^{-})_2]^{-}$. This conclusion was also supported by DFT calculations. Substituent effects on the electronic structures of the three oxidation states (neutral, cationic, and anionic) of the complexes are systematically evaluated on the basis of DFT calculations.

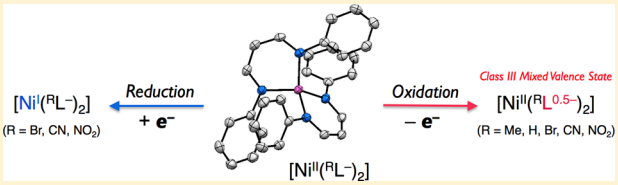

INTRODUCTION

β-Diketiminates are an important class of monoanionic bidentate ligands, which have been adopted for the synthesis of complexes with most of the metal ions in the periodic table due to their versatility in tuning the electronic as well as steric properties of the supported complexes.[1−6] Such complexes have been studied extensively as polymerization catalysts, organometallic compounds with unusual coordination geometry, and models of the metalloenzyme active sites especially for small molecule activation, where much attention has been focused on the redox and/or Lewis acidic functions of the metal center.

On the other hand, β-diketiminates have recently been shown to behave as redox noninnocent ligands in the oxidation of a nickel(II) complex as well as in the reduction of an aluminum(III) complex, providing new insights into the redox and magnetic properties of the β-diketiminate complexes.[6−8] Such ligand-based redox chemistry is possibly involved in the oxidative modifications of β-diketiminates in their complexes of copper(II), zinc(II), aluminum(III), and platinum(IV) as well.[9−12]

Transition-metal complexes supported by two redox-active ligands (or donor groups) are known to produce ligand-based mixed-valence complexes, where one-electron oxidation takes place formally at one of the supporting ligands (donor groups). In this case, the oxidized ligand as an electron acceptor is electronically linked to another intact part as an electron donor via the central metal ion, providing a good opportunity to study intramolecular electron transfer.[13−16] Typical examples of such

Received: March 22, 2014
Published: June 2, 2014

   dx.doi.org/10.1021/ic5006693 | Inorg. Chem. 2014, 53, 6159−6169

systems include transition-metal complexes with *o*-quinones,[17−19] *o*-phenylenediamines,[20,21] benzene-1,2-dithiolates,[22,23] *o*-iminophenolate,[24−27] *α*-iminopyridines,[28,29] and salens.[30−49] Such an electronic communication between the two redox centers originally started from studies of connected transition-metal centers represented by the Creutz−Taube ion, and those studies have been developed toward functional dyes and electronic materials.[50−56] Although, as stated above, the *β*-diketiminate ligands have been recently recognized to act as a redox noninnocent ligand in the bis-*β*-diketiminate complexes, detailed study on the electronic interaction between the two ligands in the mixed-valence state has yet to be accomplished due to instability of such complexes.

In this study, the redox behavior of a series of bis(*β*-diketiminate)nickel(II) complexes, $[Ni^{II}(^{R}L^{-})_2]$ ($^{R}L^{-}$, deprotonated form of ^{R}LH, see Chart 1), has been examined in detail to

Chart 1

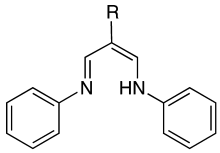

^{R}LH; R = Me, H, Br, CN, NO_2

get insights into the substituent effects on the redox noninnocence of the supporting ligands. Particular attention has been focused on the electronic communication between the two *β*-diketiminate ligands in the one-electron-oxidized mixed-valence complexes to explore the intramolecular electron transfer though a coordination bond associated with the appearance of a ligand-to-ligand intervalence charge-transfer (LLIVCT) transition band.

EXPERIMENTAL SECTION

General. Reagents and solvents used in this study, except for the ligands and nickel complexes, were commercial products of the highest available purity and further purified by standard methods, if necessary.[57] Ligands ^{R}LH (R = Me, H, Br, CN, and NO_2) were prepared according to the reported procedures.[58−61] FT-IR spectra were recorded with a Jasco FT/IR-4100. Electronic spectra were measured using a Hewlett-Packard HP8453 diode array spectrophotometer or a Jasco V-570 UV/vis/NIR spectrophotometer equipped with a Unisoku thermostated cell holder USP-203 designed for low-temperature measurements. Mass spectra were recorded with a JEOL JMS-700T Tandem MS station or a JEOL JMS-700. NMR spectra were recorded on a JEOL LMN-ECP300WB, a JEOL ECP400, a JEOL ECS400, or a Varian UNITY INOVA 600 MHz. EPR spectra were taken on a JEOL X-band spectrometer (JES-RE1XE) under non-saturating microwave power conditions (1.0 mW) operating at 9.0 GHz. The magnitude of the modulation was chosen to optimize the resolution and signal-to-noise ratio (S/N) of the observed spectrum. The *g* values were calibrated using an Mn^{2+} marker. Elemental analyses were recorded with a Perkin−Elmer or Fisons instruments EA1108 Elemental Analyzer.

Electrochemical Measurements. Cyclic voltammetric measurements were performed on a Hokuto Denko HZ-3000 or an ALS electrochemical analyzer CHI-630A in deaerated CH_2Cl_2 or THF containing 0.10 M *n*-Bu_4NClO_4 (TBAP) as supporting electrolyte. The Pt electrode was polished with BAS polishing alumina suspension, rinsed with the solvent, and dried before use. The counter electrode was a platinum wire. Redox potentials were determined with respect to a Fc/Fc^+ (Fc, ferrocene) (2.0×10^{-3} M) reference electrode. All electrochemical measurements were carried out under an atmospheric pressure of N2 in a glovebox.

X-ray Structure Determination. Each single crystal was mounted on a loop. Data from X-ray diffraction were collected at −170 °C by a VariMax with RAPID imaging plate two-dimensional area detector using graphite-monochromated Mo K*α* radiation (λ = 0.71069 Å) to $2\theta_{max}$ of 55°. All of the crystallographic calculations were performed using the Crystal Structure software package of Molecular Structure Corp. [Crystal Structure, Crystal Structure Analysis Package, version 3.8.1, Molecular Structure Corp. and Rigaku Corp. (2005)]. Structures were solved by a direct method (SIR 2008) and expanded using Fourier techniques. Non-hydrogen atoms were refined anisotropically by full-matrix least-squares on F^2. Hydrogen atoms were attached at idealized positions on carbon atoms and not refined. Crystallographic parameters are summarized in Table S1, Supporting Information.

Theoretical Calculations. Density functional theory (DFT) calculations were performed with "ultrafine" grid using Gaussian 09 (Revision D.01, Gaussian, Inc.).[62] Geometry optimizations were carried out at the long-range corrected (LC)-UOLYP level of theory[63−68] with def2SVP basis sets. We also used CAM-UB3LYP/def2SVP, LC-BP86/def2SVP, M06/def2SVP, and UM11/def2SVP levels for geometry optimization. As discussed in the text and Supporting Information, the LC-UOLYP/def2SVP method was the best among these methods. For each optimized geometry, normal coordinate analyses for energy minima were performed to confirm no imaginary frequency.[7] Graphical outputs of the computational results were generated with a ChemCraft software program.[69] Electronic excitation energies and intensities were computed by the time-dependent (TD)-DFT method with the B3LYP/TZVP basis set for Ni and the SVP basis set for other atoms (denoted as BS-I) based on optimized geometries at the LC-UOLYP/def2SVP level.[70−72] The LC-OLYP method was also used for TD-DFT calculations, but the UV−vis−NIR spectra of the B3LYP method were found to be in better agreement with the experimental spectra (see details in Supporting Information) than the LC-OLYP spectra. The B3LYP/BS-I method was used for TD-DFT studies because this method works very well for a Ni(*β*-diketiminate) system.[7,20] In each case, 85 excited states were calculated by including all one-electron excitations within an energy window of ±3 hartree with respect to the HOMO/LUMO energies. Natural charges were computed with the NBO 5.G program.[73] The integral equation formalism polarizable continuum model (PCM)[74] with radii and nonelectrostatic terms for the SMD model[75] were applied to investigate bulk solvent effects for TD-DFT calculations of CH_2Cl_2 (oxidized and neutral complex) and THF (reduced complex).

Synthesis. *$[Ni^{II}(^{Me}L^{-})_2]$.* An ethanol solution of ligand ^{Me}LH (47.3 mg, 0.20 mmol) (10 mL) was added into an ethanol solution (10 mL) of $Ni(OAc)_2{\cdot}4H_2O$ (24.9 mg, 0.10 mmol), and the mixture was heated at 40 °C for 24 h. Resulting precipitates were collected by filtration and dried to give black powder in 75%. Single crystals suitable for X-ray crystallographic analysis were obtained by slow diffusion of ethanol into a dichloromethane solution containing the complex. IR (KBr): 1578 cm^{-1} (C═N). ^{1}H NMR ($CDCl_3$, 600 MHz): δ −15.6 (s, 4 H, *p*-Ar), −11.6 (s, 8 H, *o*-Ar), 28.2 (s, 8 H, *m*-Ar), 89.1 (s, 6 H, CH_3). HRMS (FAB^+): *m*/*z* 528.1824, calcd for $C_{32}H_{30}N_4Ni$ 528.1824. Anal. Calcd for $C_{32}H_{30}N_4Ni{\cdot}CH_2Cl_2{\cdot}H_2O$: C, 62.69; H, 5.42; N, 8.86. Found: C, 62.71; H, 5.53; N, 9.05.

$[Ni^{II}(^{H}L^{-})_2]$. Ligand ^{H}LH (44.5 mg, 0.20 mmol) in ethanol (10 mL) was added into an ethanol solution (10 mL) of $Ni(OAc)_2{\cdot}4H_2O$ (24.9 mg, 0.1 mmol), and the mixture was stirred for 2 h at room temperature. Resulting precipitates were collected by filtration and dried to give red powder in 60%. Single crystals suitable for X-ray crystallographic analysis were obtained by slow diffusion of ethanol into a chloroform solution containing the complex. IR (KBr): 1574 cm^{-1} (C═N). ^{1}H NMR ($CDCl_3$, 600 MHz): δ −121.0 (s, 2 H, C*H*), −14.0 (s, 4 H, *p*-Ar), −9.6 (s, 8 H, *o*-Ar), 27.6 (s, 8 H, *m*-Ar). HRMS (FAB^+): *m*/*z* 500.1511, calcd for $C_{30}H_{26}N_4Ni$ 500.1514. Anal. Calcd for $C_{30}H_{26}N_4Ni$: C, 71.88; H, 5.23; N, 11.18. Found: C, 71.60; H, 5.24; N, 11.08.

$[Ni^{II}(^{Br}L^{-})_2]$. Ligand ^{Br}LH (30.1 mg, 0.10 mmol) in ethanol (1 mL) was added into an ethanol solution (1 mL) of $Ni(OAc)_2{\cdot}4H_2O$ (12.5

dx.doi.org/10.1021/ic5006693 | Inorg. Chem. 2014, 53, 6159−6169

mg, 0.05 mmol) and triethyamine (14 μL 0.10 mmol), and the mixture was stirred for 5 h at 50 °C. Resulting precipitates were collected by filtration and dried to give yellow powder in 76%. Single crystals suitable for X-ray crystallographic analysis were obtained by slow diffusion of methanol into a chloroform solution containing the complex. IR (KBr): 1563 cm^{-1} (C═N). ^1H NMR ($CDCl_3$, 400 MHz): δ −14.6 (s, 4 H, *p*-Ar), −10.5 (s, 8 H, *o*-Ar), 28.0 (s, 8 H, *m*-Ar). HRMS (FAB^+): *m*/*z* 655.9734, calcd for $C_{30}H_{24}Br_2N_4Ni$ 655.9721. Anal. Calcd for $C_{30}H_{24}BrN_4Ni{\cdot}H_2O$: C, 53.55; H, 3.74; N, 8.33. Found: C, 53.56; H, 3.92; N, 8.39.

[Ni^{II}(^{CN}L$^-$)$_2$]. The compound was prepared by the method described for [Ni^{II}(^{Me}L$^-$)$_2$] (85% yield). Single crystals suitable for X-ray crystallographic analysis were obtained by slow diffusion of ethanol into a dichloromethane solution containing the complex. IR (KBr): 2206 (C≡N), 1605 cm^{-1} (C═N). ^1H NMR ($CDCl_3$, 600 MHz): δ −10.9 (s, 4 H, *p*-Ar), −6.2 (s, 8 H, *o*-Ar), 25.9 (s, 8 H, *m*-Ar). HRMS (FAB^+): *m*/*z* 551.1505, calcd for $C_{32}H_{25}N_6Ni$ 551.1494. Anal. Calcd for $C_{32}H_{24}N_6Ni$: C, 69.72; H, 4.39; N, 15.24. Found: C, 69.53; H, 4.34; N, 15.14.

[Ni^{II}(^{NO2}L$^-$)$_2$]. The compound was prepared by the method described for [Ni^{II}(^{Me}L$^-$)$_2$] (73% yield). Single crystals suitable for X-ray crystallographic analysis were obtained by slow diffusion of ethanol into a dichloromethane solution containing the complex. IR (KBr) 1600 (C═N); 1582, 1528, 1489, 1277 cm^{-1} (NO_2). ^1H NMR ($CDCl_3$, 600 MHz): δ −9.2 (s, 4 H, *p*-Ar), −3.8 (s, 8 H, *o*-Ar), 24.9 (s, 8 H, *m*-Ar). HRMS (FAB^+): *m*/*z* 591.1304, calcd for $C_{30}H_{25}N_6NiO_4$ 591.1291. Anal. Calcd for $C_{30}H_{24}N_6NiO_4$: C, 60.94; H, 4.09; N, 14.21. Found: C, 60.89; H, 4.11; N, 14.03.

[Ni^{II}(^{H}L$^{0.5•-}$)$_2$](SbF$_6$). $AgSbF_6$ (98%, 3.5 mg, 0.010 mmol) in CH_2Cl_2 (0.2 mL) was added to a CH_2Cl_2 solution (0.4 mL) of [Ni^{II}(^{H}L$^-$)$_2$] (5.2 mg, 0.010 mmol) with stirring at −40 °C. The solution was stirred at −40 °C for 1 h, and [Ni^{II}(^{H}L$^{0.5•-}$)$_2$](SbF_6) was obtained as yellow crystals by slow diffusion of diethyl ether into the reaction solution at −40 °C. MS (ESI^+): *m*/*z* 500.39, calcd for $C_{30}H_{26}N_4Ni$ 500.15.

RESULTS AND DISCUSSION

Synthesis and Characterization of [Ni^{II}(^{R}L$^-$)$_2$]. Nickel complexes [Ni^{II}(^{R}L$^-$)$_2$] were prepared by treating the neutral ligand ^{R}LH (R = Me, H, Br, CN, and NO_2, Chart 1) with $Ni(OAc)_2{\cdot}4H_2O$ in ethanol. The crystal structure of the nickel complex of ^{H}L$^-$ is presented in Figure 1 as a typical example,

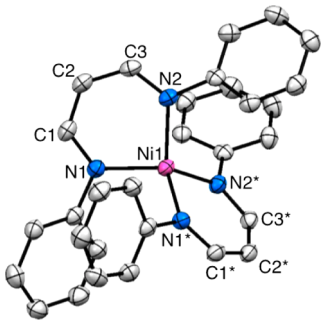

Figure 1. ORTEP drawing of [Ni^{II}(^{H}L$^-$)$_2$] showing 50% probability thermal ellipsoids. Hydrogen atoms are omitted for clarity.

and those of the other complexes with ^{R}L$^-$ (R = Me, Br, CN, and NO_2) are given in the Supporting Information (Figures S1−S4). Selected bond lengths and bond angles as well as the angles of least-squares planes between the two six-membered chelate rings (θ) are summarized in Table 1.

All neutral nickel(II) complexes [Ni^{II}(^{R}L$^-$)$_2$] exhibit a similar distorted tetrahedral geometry ligated by two β-diketiminate ligands. The twist angles of the two nearly planar six-membered chelate rings (θ) are 69.85−73.11°, which are similar to that of the nickel complex supported by L2$^-$ (for the ligand structure, see Chart 2), θ = 72.3°, but smaller as compared to that of the L1 complex, θ = 86.45° (Chart 2), previously reported.[7,76] The averaged Ni−N distances of [Ni^{II}(^{R}L$^-$)$_2$] are 1.934−1.954 Å, which are also close to those of the nickel complexes of L1$^-$ and L2$^-$ (1.958 and 1.949(1) Å, respectively).[7,76] Ni−N distances slightly decrease from 1.9557(12) to 1.937(3) Å as the electron-donating nature of substituent R increases (Table 1).

All nickel(II) complexes [Ni^{II}(^{R}L$^-$)$_2$] exhibit ^1H NMR signals in the paramagnetic region (see Experimental Section), indicating a high-spin state (*S* = 1) of the metal center, as in the case of other bis(β-diketiminate)nickel(II) complexes with a distorted tetrahedral geometry reported in the literature.[1,7,77]

Electrochemistry. The redox behavior of the neutral complexes has been examined by cyclic voltammetry (CV) in CH_2Cl_2 (for the oxidation) and THF (for the reduction) containing 0.10 M TBAP (tetra-*n*-butylammonium perchlorate) as the supporting electrolyte under N2 atmosphere at 25 °C. Cyclic voltammograms are presented in Figures S5, S6, and S7, Supporting Information, and redox potentials are summarized in Table 2.

All complexes exhibit a reversible redox couple due to one-electron oxidation of the complex ($E^{ox}_{1/2}$) in CH_2Cl_2, which clearly shows a negative shift as the electron-donating nature of R increases; 0.90 (NO_2) > 0.75 (CN) > 0.27 (Br) > 0.08 (H) > −0.05 (Me) (vs Fc/Fc^+, Table 2 and Figure S5, Supporting Information). Thus, the difference in $E^{ox}_{1/2}$ between [Ni^{II}(^{NO2}L$^-$)$_2$] and [Ni^{II}(^{Me}L$^-$)$_2$] reaches about 1 V. A cyclic voltammogram of [Ni^{II}(^{H}L$^-$)$_2$] scanned up to 1.0 V vs Fc/Fc^+ is also shown in the Supporting Information (Figure S6), which shows the presence of a second oxidation of the complex around 0.89 V, albeit the reduction wave does not appear clearly. The nickel(II) complex of L2$^-$ (see Chart 2) was reported to exhibit $E^{ox}_{1/2}$ at −0.33 V vs Fc/Fc^+, which is significantly more negative as compared to those of [Ni^{II}(^{R}L$^-$)$_2$]. This is probably due to electron donation by the four methyl substituents in L2$^-$ (Chart 2).

Electrochemical reduction of [Ni^{II}(^{R}L$^-$)$_2$] was examined in THF as shown in Figure S7, Supporting Information, and Table 2. [Ni^{II}(^{R}L$^-$)$_2$] with R = NO_2, CN, and Br exhibited a reversible redox couple due to one-electron reduction of the complexes at $E^{red}_{1/2}$ = −1.28, −1.64, and −1.89 V vs Fc/Fc^+, respectively. Such reduction has not been reported with nickel complexes of L1$^-$ and L2$^-$.[7,59] Reversibility of the redox couple of [Ni^{II}(^{R}L$^-$)$_2$] with R = H and Me, however, became poorer with increasing electron-donating ability of substituents, and the reduction of [Ni^{II}(^{Me}L$^-$)$_2$] was completely irreversible (Figure S7, Supporting Information). Nonetheless, it is apparent that $E^{red}_{1/2}$ becomes more negative as the electron-donating nature of R increases.

Formation and Characterization of One-electron-Oxidized Complexes. Judging from $E^{ox}_{1/2}$ listed in Table 2, [Ni^{II}(^{R}L$^-$)$_2$] with R = Me, H, and Br can be oxidized by $AgSbF_6$ ($E^{red}_{1/2}$ = 0.65 V vs Fc/Fc^+),[78] whereas [Ni^{II}(^{R}L$^-$)$_2$] with R = CN and NO_2 needs a stronger oxidant such as [$Ru^{III}(bpy)_3$]-(PF_6)$_3$ (bpy = 2,2′-bipyridine) ($E^{red}_{1/2}$ = 1.03 V vs Fc/Fc^+)[79] to be oxidized. UV−vis spectral changes for the redox titration of [Ni^{II}(^{H}L$^-$)$_2$] with $AgSbF_6$ in CH_2Cl_2 at 30 °C are shown in Figure 2A. The absorption band at 395 nm (ε = 35 400 M^{-1} cm^{-1}) due to [Ni^{II}(^{H}L$^-$)$_2$] decreases with concomitant increase in the absorption bands at 355 (ε = 35 300 M^{-1} cm^{-1}) and 620 nm (ε = 13 300 M^{-1} cm^{-1}) with clear isosbestic points at 373

dx.doi.org/10.1021/ic5006693 | Inorg. Chem. 2014, 53, 6159−6169

Table 1. Selected Bond Lengths (Angstroms), Bond Angles (degrees), and Angles of Least Square Planes between Six-Membered Chelate Rings (degrees)

Ni complex	M−N1	M−N2	N1−C1	C1−C2	C2−C3	C3−N2	N1−M−N2	M−N1−C1	M−N2−C3	θ^a
$[Ni^{II}(^{Me}L^-)_2]$	1.937(3)	1.934(2)	1.327(3)	1.394(4)	1.394(4)	1.332(3)	94.07(9)	125.07(19)	124.50(19)	73.11
$[Ni^{II}(^{H}L^-)_2]$	1.938(3)	1.955(3)	1.316(5)	1.390(6)	1.397(6)	1.315(5)	93.87(13)	125.0(3)	125.2(3)	70.66
$[Ni^{II}(^{Br}L^-)_2]$	1.956(5)	1.952(5)	1.315(7)	1.398(7)	1.388(7)	1.342(7)	94.36(18)	125.1(4)	124.5(4)	71.13
$[Ni^{II}(^{CN}L^-)_2]$	1.9489(13)	1.9534(13)	1.319(3)	1.404(2)	1.414(2)	1.316(2)	93.89(5)	124.92(10)	126.07(10)	69.85
$[Ni^{II}(^{NO2}L^-)_2]$	1.9557(12)	1.9487(11)	1.3149(16)	1.4097(19)	1.406(2)	1.3118(17)	94.75(5)	125.17(10)	124.87(10)	71.07
$[Ni^{II}(^{H}L^{0.5\bullet-})_2]^+$	1.8914(16)	1.8914(16)	1.323(3)	1.388(3)	1.388(3)	1.323(3)	95.46(7)	124.90(13)	124.90(13)	73.09

[a]Twist angle between the two six-membered chelate rings.

Chart 2

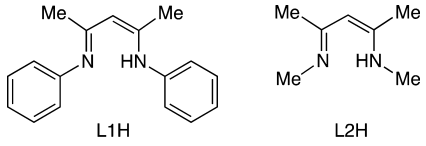

and 450 nm. The spectral change was completed when an equimolar amount of $AgSbF_6$ was added as shown in Figure 2B. This clearly demonstrated that the process was one-electron oxidation of $[Ni^{II}(^{H}L^-)_2]$.

Notably, the one-electron-oxidized complexes of $[Ni^{II}(^{R}L^-)_2]$ were stable even at room temperature in contrast to the instability of the one-electron-oxidized complex of $[Ni^{II}(L2^-)_2]$.[7] This may be due to the $\pi-\pi$ stacking interaction between the two phenyl substituents in our ligand system ($^{R}L^-$, see Chart 1), which is absent in ligand $L2^-$ (see Chart 2), as discussed below. It should be also noted that the oxidation product showed a broad and relatively intense absorption band in the near-IR region (centered at λ_{max} = 2150 nm, ε = 1530 M^{-1} cm^{-1}) attributable to a ligand-to-ligand intervalence charge transfer (LLIVCT) transition (inset of Figure 2A). This suggests that the one-electron oxidation occurred at the ligand moiety to give a nickel(II) organic radical complex as in the case of the L2 ligand system.[7] In fact, the final spectrum shown in Figure 2A (red line) is similar to the spectrum of the one-electron-oxidized complex of $[Ni^{II}(L2^-)_2]$, exhibiting $\pi-\pi^*$ transition bands at ∼300 and 591 nm, although the NIR spectrum of the L2 complex was not reported previously.[7] Thus, the one-electron oxidation product can be best described as a mixed-valence Ni^{II} complex having an oxidized ligand.

Depending on the extent of electronic interactions between two redox centers, the mixed-valence state can be classified into three categories, classes I, II, and III, as proposed by Robin and Day.[13] In class I mixed-valence compounds, no electron transfer occurs when two bridged redox centers are far apart or when they do not have interaction because of symmetry or spin forbiddeness. In class II mixed-valence compounds, two redox centers have detectable electronic interaction and electron transfer occurs between the redox centers. In class III mixed-valence compounds, two redox centers have strong electronic interaction when delocalization occurs and the formal charge on each redox center is averaged. Class III mixed-valence compounds are distinct from class II compounds in delocalization of the unpaired electron as a consequence of disappearance of the activation barrier for electron transfer. In addition to the typical Robin−Day classification, a number of recent studies have demonstrated the existence of somewhat complicated systems exhibiting an intermediate behavior between class II and class III, which are now categorized as the borderline class II−III.[47,80−84]

According to the Marcus−Hush theory, the bandwidth at half-height ($\Delta\nu_{1/2}$, cm^{-1}) for the IVCT transition from a class II mixed-valence system can be predicted by the following equation: $\Delta\nu_{1/2} = (16RT(\ln 2)\nu_{max})^{1/2}$, where R is the gas constant, T is the absolute temperature (K), ν_{max} is the band maximum (cm^{-1}), and $16RT \ln 2$ takes a value of 2310 cm^{-1} at 298 K.[14,15] When the experimental $\Delta\nu_{1/2}$ value ($\Delta\nu_{1/2,exp}$) is equal to or broader at the theoretical value ($\Delta\nu_{1/2,theo}$), the electronic structure is regarded as class II. When $\Delta\nu_{1/2,exp}$ is smaller than $\Delta\nu_{1/2,theo}$, the mixed-valence system is assigned as class III or borderline class II−III. In our present system, all of $\Delta\nu_{1/2,exp}$ are smaller than $\Delta\nu_{1/2,theo}$, indicating that the oxidized complex can be assigned as class III. Thus, the electronic configuration of the oxidized complex is best described as $[Ni^{II}(^{H}L^{0.5\bullet-})_2]^+$, where the generated radical spin is completely delocalized between the two ligands (Table 3).

The stability of the mixed-valence state toward disproportionation can be estimated from the comproportionation constant (K_c) determined from the difference of the first and second oxidation potential of $[Ni^{II}(^{R}L^-)_2]$ (ΔE) using the following equation: $K_c = \exp(F\Delta E/RT)$. For the R = H derivative, K_c was determined to be 3.7×10^{13} from the ΔE value of 0.76 given by the comparison of peak potentials of the oxidation waves, which clearly indicates the large stability of the mixed-valence state.

An EPR spectrum of $[Ni^{II}(^{H}L^{0.5\bullet-})_2]^+$ (g_1 = 2.301, g_2 = 2.134, g_3 = 2.027) shown in Figure 3 is similar to that of the one-electron-oxidized nickel(II) complex of ligand L2 (S = 1/2).[7]

Table 2. Electrochemical Data of Oxidation and Reduction of $[Ni^{II}(^{R}L^-)_2]$

	oxidation[a]			reduction[b]		
Ni complex	E_{ap}/V[c]	E_{cp}/V[c]	$E^{ox}_{1/2}$/V[c]	E_{ap}/V[c]	E_{cp}/V[c]	$E^{red}_{1/2}$/V[c]
$[Ni^{II}(^{Me}L^-)_2]$	−0.01	−0.09	−0.05		−2.42	
$[Ni^{II}(^{H}L^-)_2]$	0.13	0.02	0.08	−2.07	−2.26	−2.16
$[Ni^{II}(^{Br}L^-)_2]$	0.32	0.22	0.27	−1.80	−1.99	−1.89
$[Ni^{II}(^{CN}L^-)_2]$	0.80	0.70	0.75	−1.55	−1.73	−1.64
$[Ni^{II}(^{NO2}L^-)_2]$	0.96	0.84	0.90	−1.20	−1.37	−1.28

[a]in CH_2Cl_2. [b]Measured in THF due to instability of CH_2Cl_2 in the negative scan. [c]vs Fc/Fc^+.

dx.doi.org/10.1021/ic5006693 | Inorg. Chem. 2014, 53, 6159−6169

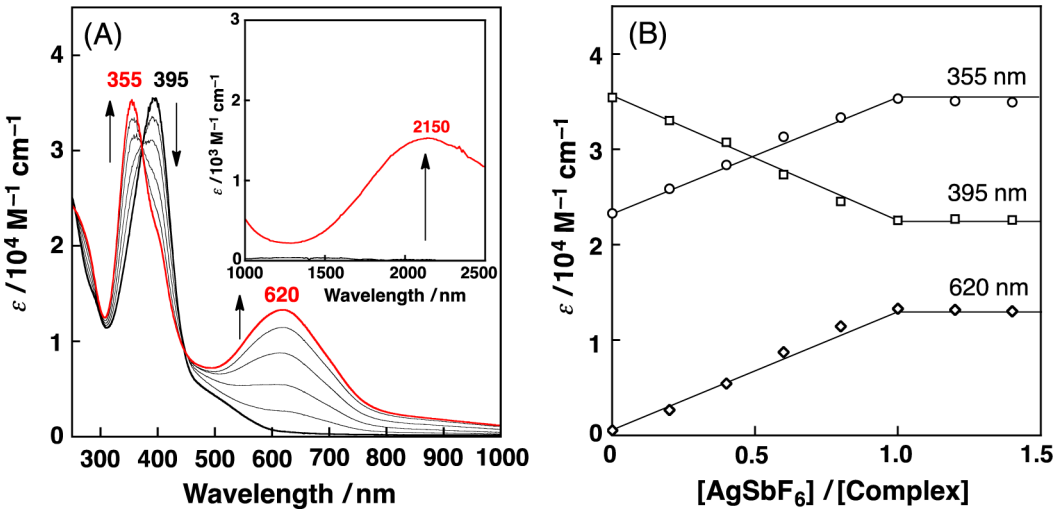

Figure 2. (A) UV−vis−NIR spectral change for the titration of $[Ni^{II}(^{H}L^{-})_2]$ (5.9×10^{-5} M) with $AgSbF_6$ (0−8.3×10^{-5} M) in CH_2Cl_2 at 30 °C. (Inset) Expanded spectra in the NIR region. (B) Plots of the absorbance at 355, 395, and 620 nm against the molar ratio of $[AgSbF_6]/[Ni^{II}(^{H}L^{-})_2]$.

Table 3. Experimental ($\Delta\nu_{1/2,exp}$) and Theoretical Values ($\Delta\nu_{1/2,theo}$) of $[Ni^{II}(^{R}L^{0.5\bullet-})_2]^+$

Ni complex	$\Delta\nu_{1/2,exp}/cm^{-1}$ [a]	$\Delta\nu_{1/2,theo}/cm^{-1}$
$[Ni^{II}(^{Me}L^{0.5\bullet-})_2]^+$	2260	3140
$[Ni^{II}(^{H}L^{0.5\bullet-})_2]^+$	2200	3290
$[Ni^{II}(^{Br}L^{0.5\bullet-})_2]^+$	2300	3080
$[Ni^{II}(^{CN}L^{0.5\bullet-})_2]^+$	2180	3060
$[Ni^{II}(^{NO2}L^{0.5\bullet-})_2]^+$	2130	3160

[a]Determined by modeling the band with a symmetric Gaussian function.

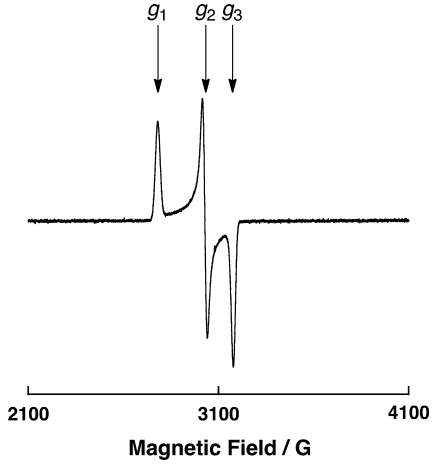

Figure 3. EPR spectrum of $[Ni^{II}(^{H}L^{0.5\bullet-})_2]^+$ in CH_2Cl_2/CH_3CN (v:v = 3:1) at −196 °C.

Thus, the spin on the radical ligand (S_L = 1/2) strongly antiferromagnetically coupled to a high-spin Ni^{II} ion (S_{Ni} = 1) to give an overall doublet ground state (S_T = 1/2) as reported previously.[7] Note that these g values were shifted from the free electron value (g = 2.002), which is consistent with the dominant Ni character in the SOMO in this complex as in the case of [Ni(Salpn)]SbF_6 complex (Salpn = *N*,*N*′-bis(3,5-di-*tert*-butylsalicylidene)-1,3-propane-diamine), which is characterized as a class III complex.[85]

In contrast to the instability of the reported mixed-valence Ni^{II} complex of L2,[7] our complex $[Ni^{II}(^{H}L^{0.5\bullet-})_2]^+$ has enough stability, allowing us to determine the crystal structure as shown in Figure 4. Selected bond lengths and bond angles as well as

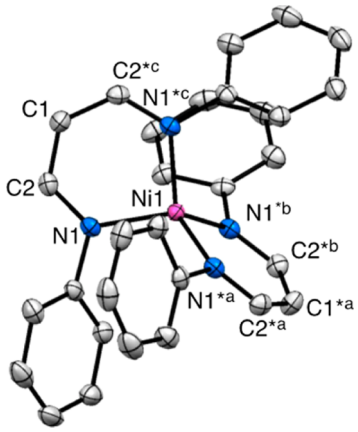

Figure 4. ORTEP drawing of $[Ni^{II}(^{H}L^{0.5\bullet-})_2]^+$ (one-electron-oxidized complex) showing 50% probability thermal ellipsoids. Hydrogen atoms are omitted for clarity.

the angles of least-squares planes between the two six-membered chelate rings are included in Table 1. The crystal structure exhibits a centrosymmetry, indicating that the four Ni−N bonds and the four C−N−Ph moieties are equivalent, consistent with the assignment as the class III complex (vide ante).

The Ni−N distances (1.8914 Å) of $[Ni^{II}(^{H}L^{0.5\bullet-})_2]^+$ become shorter as compared to those of $[Ni^{II}(^{H}L^{-})_2]$ (averaged value, 1.947 Å), whereas the twist angle θ (73.09°) of the former is larger than that of the latter (70.66°). These structural features around the metal center of the one-electron-oxidized complex are consistent with those predicted by the DFT calculation for the L2 complex.[7] Interestingly, $\pi-\pi^{\bullet+}$ interaction was found between the two phenyl groups attached on the nitrogen atoms of different β-diketiminate ligands (Figure 5). The distance between the two phenyl groups gets closer (3.4 Å) to have a typical value for such interaction, and their alignment is more parallel as compared to that in the corresponding neutral complex.[86−90] The higher thermal stability of $[Ni^{II}(^{H}L^{0.5\bullet-})_2]^+$ as compared to $[Ni^{II}(L2^{0.5\bullet-})_2]^+$ can be attributed to such an

dx.doi.org/10.1021/ic5006693 | Inorg. Chem. 2014, 53, 6159−6169

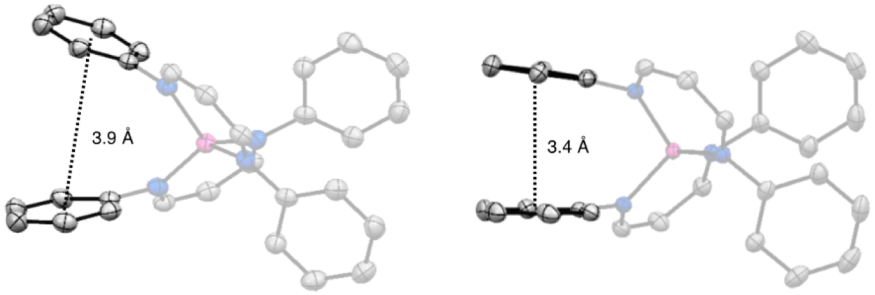

Figure 5. Comparison of the steric relation between the two phenyl substituents in $[Ni^{II}(^{H}L^{-})_2]$ (left) and $[Ni^{II}(^{H}L^{0.5\bullet-})_2]^+$ (right).

intramolecular $\pi-\pi^{\bullet+}$ stacking interaction. DFT calculations also suggested the presence of such an interaction in the one-electron-oxidized complex (vide infra). The bond lengths between the nickel ion and the nitrogen atoms get slightly shorter (0.056 Å) despite the fact that the electron density of the β-diketiminate ligands decreases. This may be attributed to formation of a stronger bonding interaction between the unpaired electrons on the nickel ion and the ligand radical. The bond lengths at the β-diketiminate backbone (N_1-C_1, C_1-C_2, C_2-C_3, C_3-N_3) were hardly changed upon oxidation (differences are up to 0.02 Å). A redox-active molecular orbital of the five-membered β-diketiminate framework is proposed to be π orbital with nonbonding character.[7] This is also confirmed by DFT calculation (vide infra).

Electronic absorption spectra as well as EPR spectra of other one-electron-oxidized complexes $[Ni^{II}(^{R}L^{0.5\bullet-})_2]^+$ (R = Me, Br, CN, and NO_2) were also obtained as summarized in Table 4.

Table 4. UV–Vis and EPR Data of $[Ni^{II}(^{R}L^{0.5\bullet-})_2]^+$

	UV–vis		EPR parameter		
Ni complex	λ_{max}/nm	λ_{max}/nm	g_1	g_2	g_3
$[Ni^{II}(^{Me}L^{0.5\bullet-})_2]^+$	577	2300	2.287	2.129	2.028
$[Ni^{II}(^{H}L^{0.5\bullet-})_2]^+$	620	2150	2.301	2.134	2.027
$[Ni^{II}(^{Br}L^{0.5\bullet-})_2]^+$	627	2400	2.315	2.145	2.030
$[Ni^{II}(^{CN}L^{0.5\bullet-})_2]^+$	723	2150	2.348	2.150	2.029
$[Ni^{II}(^{NO2}L^{0.5\bullet-})_2]^+$	756	1977	2.360	2.158	2.030

As mentioned above, $[Ni^{II}(^{Me}L^{0.5\bullet-})_2]^+$ and $[Ni^{II}(^{Br}L^{0.5\bullet-})_2]^+$ were generated by oxidation with $AgSbF_6$, whereas $[Ni^{II}(^{CN}L^{0.5\bullet-})_2]^+$ and $[Ni^{II}(^{NO2}L^{0.5\bullet-})_2]^+$ were generated using a stronger oxidant $[Ru^{III}(bpy)_3](PF_6)_3$. The former two complexes (R = Me and Br) are stable at 30 °C as in the case of $[Ni^{II}(^{H}L^{0.5\bullet-})_2]^+$, whereas the latter two complexes (R = CN and NO_2) could be generated only at lower temperature (−20 °C) due to their lower thermal stability.

The appearance of the $\pi-\pi^*$ and LLIVCT bands in the electronic absorption spectra (Figures S12–S15, Supporting Information) as well as the EPR spectra due to $S = 1/2$ species (Figures S8–S11, Supporting Information) clearly demonstrate that one-electron oxidation of all other complexes (R = Me, Br, CN, and NO_2) occurs at the supporting ligand, affording similar type complexes in the class III mixed-valence category $[Ni^{II}(^{R}L^{0.5\bullet-})_2]^+$, although the oxidation potentials of the starting complexes are quite different. Notably, the $\pi-\pi^*$ bands in the visible region exhibit a red shift as the electron-withdrawing nature of R increases; λ_{max} = 577, 620, 627, 723, and 756 nm for R = Me, H, Br, CN, and NO_2, respectively (see Figures 2 and S12–S15, Supporting Information). The electron-withdrawing substituents may lower the energy level of the ligand-based MOs as demonstrated by the positive shift of $E^{ox}_{1/2}$ (Table 2), which enhances the overlap with the d orbitals of the metal center.

One-Electron Reduction of $[Ni^{II}(^{R}L^{-})_2]$. Since $[Ni^{II}(^{NO2}L^{-})_2]$, $[Ni^{II}(^{CN}L^{-})_2]$, and $[Ni^{II}(^{Br}L^{-})_2]$ exhibited a reversible redox couple in the negative sweep of the CV measurements (Figure S7, Supporting Information), chemical reduction of the complexes was also examined by UV–vis and EPR spectra. A spectral change for the reduction of $[Ni^{II}(^{CN}L^{-})_2]$ with an equimolar amount of decamethylcobaltocene ($CoCp^*_2$, E^{ox} = −1.91 V vs Fc/Fc^+)[91] in THF at 30 °C is shown in Figure 6, where new absorption bands at 348 (43

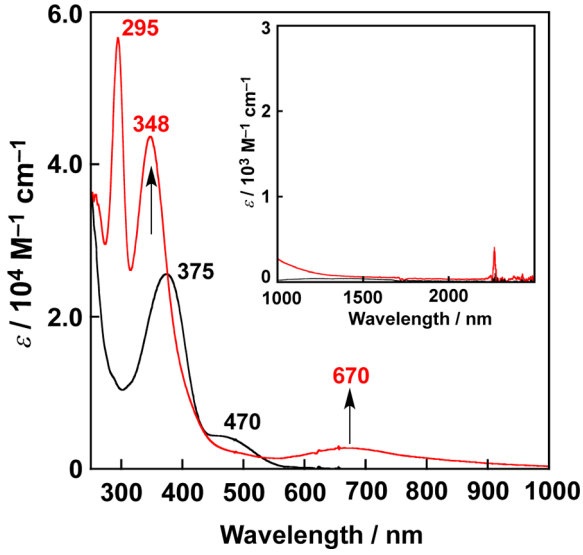

Figure 6. UV–vis–NIR spectral change for the reduction of $[Ni^{II}(^{CN}L^{-})_2]$ (2.5×10^{-5} M) (black) with $CoCp^*_2$ (2.5×10^{-5} M) in THF at 30 °C.

700 M^{-1} cm^{-1}) and 670 nm (2760 M^{-1} cm^{-1}) due to the reduced product rapidly appeared together with the absorption band at 295 nm (ε = 56 700 M^{-1} cm^{-1}) due to $CoCp^*_2{}^+$. Further addition of $CoCp^*_2$ did not alter the final spectrum, demonstrating that one-electron-reduced complex was formed with 1:1 stoichiometry. A similar spectral change was observed in the reduction of $[Ni^{II}(^{NO2}L^{-})_2]$ with $CoCp^*_2$ as shown in Figure S16, Supporting Information. In the case of $[Ni^{II}(^{Br}L^{-})_2]$ (E^{red} = −1.89 V), an excess amount of $CoCp^*_2$ was needed to complete the reduction reaction, since the electron transfer between $[Ni^{II}(^{Br}L^{-})_2]$ and $CoCp^*_2$ was in equilibrium (Figure S17, Supporting Information).

The reduced complexes exhibit broad absorption band(s) in the visible region (λ_{max} = 670 (ε = 2760 M^{-1} cm^{-1}) and 650

dx.doi.org/10.1021/ic5006693 | Inorg. Chem. 2014, 53, 6159–6169

nm (7000 M^{-1} cm^{-1}) but did not afford any absorption band in the NIR region (above 1000 nm), in contrast to the one-electron-oxidized species. Thus, one-electron reduction of the neutral complex $[Ni^{II}(^{R}L^{-})_2]$ may occur at the metal center to generate a nickel(I) complex $[Ni^{I}(^{R}L^{-})_2]^{-}$. This has been confirmed by the EPR spectra shown in Figures 7 (for

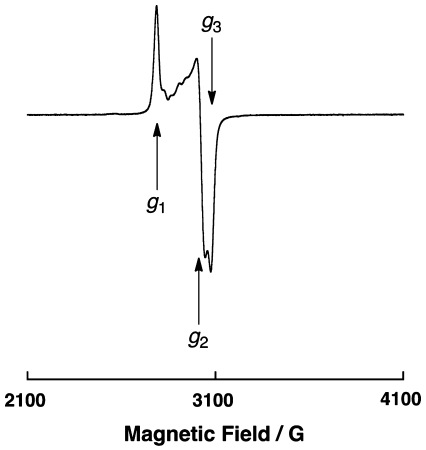

Figure 7. EPR spectrum of $[Ni^{I}(^{CN}L^{-})_2]^{-}$ in THF at −196 °C generated by the reduction of $[Ni^{II}(^{CN}L^{-})_2]$ with $CoCp^{*}_2$; g_1 = 2.31, g_2 = 2.13, and g_3 = 2.09.

$[Ni^{I}(^{CN}L^{-})_2]^{-}$) and S18, Supporting Information (for $[Ni^{I}(^{NO2}L^{-})_2]^{-}$), which are attributable to the nickel(I) species having d^9 electronic configuration.[92−97] This conclusion was also supported by DFT calculations (Table 5).

DFT Calculations. Several DFT methods were tested using the X-ray structures of $[Ni^{II}(^{R}L^{-})_2]$ (R = H, Me, Br, CN, NO_2) and $[Ni^{II}(^{H}L^{0.5\bullet-})_2]^{+}$. As shown in Table S2, Supporting Information, among several DFT methods used for a triplet $[Ni^{II}(^{H}L^{-})_2]$ complex, the LC-OLYP/def2SVP method has the smallest root-mean square deviation (RMSD) value of 0.11 Å for the corresponding heavy atom positions between the X-ray structures and DFT-optimized structures. However, the LC-OLYP method combined with the larger def2TZVP basis sets resulted in no significant improvement. Thus, the LC-OLYP/def2SVP method was employed for calculations of other Ni complexes, $[Ni^{II}(^{R}L^{-})_2]$ (R = Me, Br, CN, and NO_2) and $[Ni^{II}(^{H}L^{0.5\bullet-})_2]^{+}$, as shown in Tables S3−S7, Supporting Information, the optimized structures of which are in good agreement with the X-ray structures.

Electronic Configurations. Mulliken spin distributions and natural charges of all complexes in the cationic, neutral, and anionic oxidation states are summarized in Table 5.

In the neutral triplet complexes $[Ni^{II}(^{R}L^{-})_2]$ (S = 1), Mulliken spin densities of Ni are 1.56−1.63 and those of the ligands are 0.19−0.22, clearly demonstrating that the neutral complexes have essentially a Ni^{II} d^8 character and that unpaired electrons are slightly delocalized onto the two β-diketiminate ligands. Electronic charges of Ni are 0.83−0.91 and those of the ligands are −0.42 ∼ −0.46, indicating that the Ni−ligand coordination bonds are polarized. Electron-withdrawing substituents like CN and NO_2 make the electronic charges of Ni slightly more positive as compared with the case of R = H. The high-spin d^8 character of Ni^{II} was confirmed with the MO analysis of Ni d orbitals as indicated in Figure S19, Supporting Information, where unpaired α-spin electrons are accommodated in the d_{xy} and d_{zx} orbitals.

In the oxidized complexes $[Ni^{II}(^{R}L^{0.5\bullet-})_2]^{+}$ with doublet spin state (S = 1/2), the Ni centers still keep a largely positive spin density as 1.20−1.36 and exhibit a high-spin d^8 character as shown in Figure 8. On the other hand, positive electronic charges (from +0.11 to +0.18) are developed on the supporting ligands upon one-electron oxidation, whereas the electronic charges on the nickel center are similar (from +0.78 to +0.84) to those of the neutral complexes. Upon oxidation, αHOMO (π_L) in the neutral complex $[Ni^{II}(^{R}L^{-})_2]$ loses one electron to become αLUMO (π_L) in the oxidized complex (see Figures 8 and S19, Supporting Information). These results unambiguously demonstrate that the ligand oxidation occurs in the cationic complexes. To generate a doublet species, Ni^{II} and the ligand radial is an antiferromagnetic couple as discussed above. This is supported by the opposite spin densities between the ligands (from −0.13 to −0.18) and the Ni^{II} center (from +1.20 to +1.36). The antiferromagnetic coupling is related to the delocalized nature of the SOMOs of the oxidized complex (see two unpaired MOs $d_{yz}(\alpha)$ and $\pi_L(\beta)$ in Figure 8A).[98] In the oxidized complex $[Ni^{II}(^{H}L^{0.5\bullet-})_2]^{+}$, the Ni d_{xy} orbital and 2p orbital of the nitrogen atoms of the ligands are overlapped (Figure 8A). Average Ni−N distances of the oxidized complexes are shorter than the neutral complexes by 0.04 Å. This coordination sphere contraction was also reported in the Ni−phenoxyl[99] and Ni−bis(β-diketiminate) complexes.[7] As shown in Figure 8B, the $\pi_L(\alpha)$ orbital on the ligand of the neutral complex consists of a nonbonding π orbital of the β-diketiminate moiety and the phenyl group, which nicely explains the ignorable structural change of the β-diketiminate backbone upon one-electron oxidation of the complex (vide ante). The ligand moiety of the $\pi_L(\alpha)$ orbital has out-of-phase overlap with the nickel d orbital, resulting in the contracted Ni−N distance accompanied by one-electron oxidation of the $[Ni^{II}(^{R}L^{-})_2]$ complex (see Table 1).

Closely looking over the contour mapping of the electron density of αHOMO (SOMO) of $[Ni^{II}(^{H}L^{0.5\bullet-})_2]^{+}$, the appearance of overlapping of orbitals on facing phenyl rings can be confirmed (Figure 9). This is consistent with the

Table 5. Mulliken Spin Densities and Natural Charges (in Parentheses) of $[Ni^{II}(^{R}L^{0.5\bullet-})_2]^{+}$, $[Ni^{II}(^{R}L^{-})_2]$, and $[Ni^{I}(^{R}L^{-})_2]^{-}$ at the UB3LYP(SMD)/BS-I//LC-UOLYP/def2SVP Level

	$[Ni^{II}(^{R}L^{0.5\bullet-})_2]^{+}$		$[Ni^{II}(^{R}L^{-})_2]$		$[Ni^{I}(^{R}L^{-})_2]^{-}$	
R	Ni	ligand	Ni	ligand	Ni	ligand
Me	1.20 (0.78)	−0.14 (0.11)	1.57 (0.85)	0.21 (−0.42)	0.95 (0.45)	0.02 (−0.72)
H	1.25 (0.79)	−0.13 (0.10)	1.56 (0.83)	0.22 (−0.42)	0.96 (0.45)	0.02 (−0.73)
Br	1.36 (0.82)	−0.18 (0.09)	1.56 (0.84)	0.22 (−0.42)	0.96 (0.46)	0.02 (−0.73)
CN	1.33 (0.84)	−0.16 (0.08)	1.62 (0.90)	0.19 (−0.45)	0.96 (0.47)	0.02 (−0.74)
NO_2	1.29 (0.84)	−0.15 (0.08)	1.63 (0.91)	0.19 (−0.46)	0.95 (0.48)	0.02 (−0.74)

dx.doi.org/10.1021/ic5006693 | Inorg. Chem. 2014, 53, 6159−6169

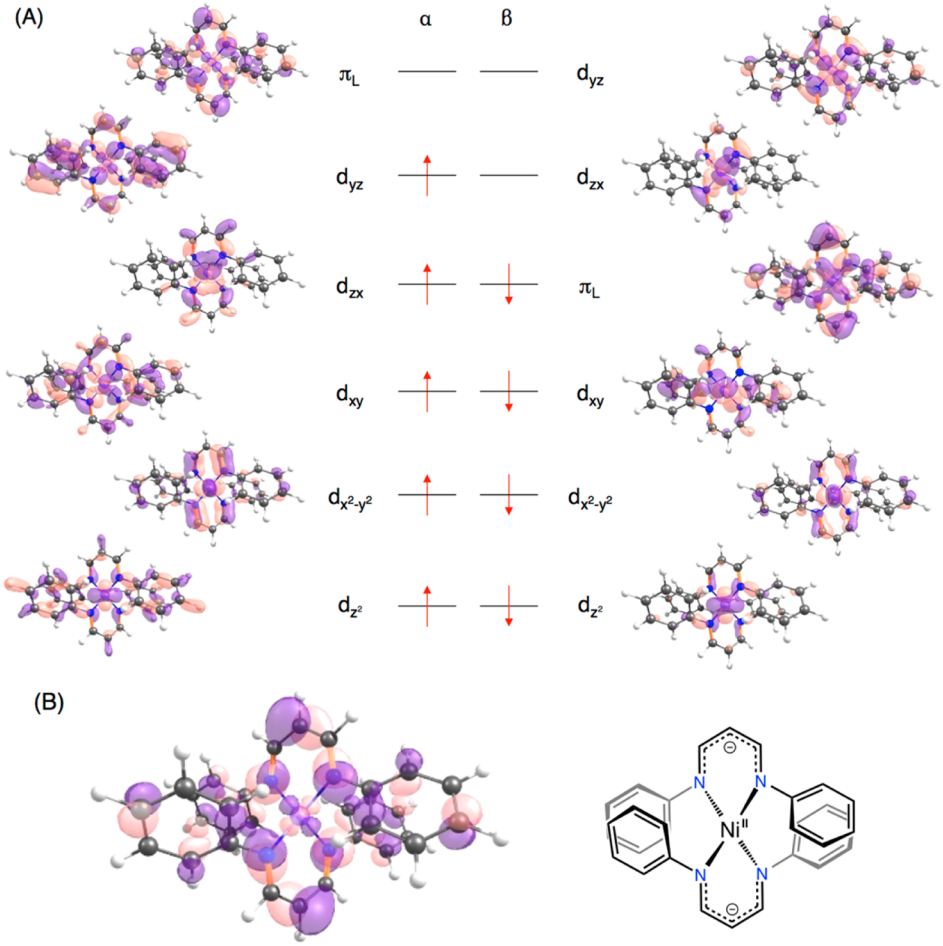

Figure 8. (A) Representative Ni d and ligand orbitals of $[Ni^{II}(^{H}L^{0.5\bullet-})_2]^+$. (B) αHOMO of $[Ni^{II}(^{H}L^{-})_2]$ (left) and its schematic structure (right).

contiguity of the phenyl rings concomitant with one-electron oxidation of the complex.

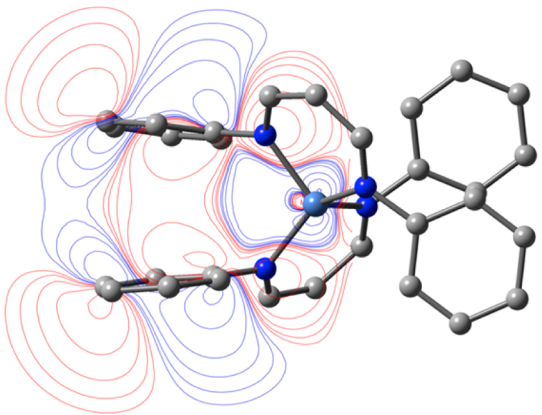

Figure 9. Contour map of the electron density of the SOMO of $[Ni^{II}(^{H}L^{0.5\bullet-})_2]^+$.

In the reduced complexes $[Ni^{I}(^{R}L^{-})_2]^-$, positive spin densities of Ni are reduced to 0.95−0.96 whereas the spin densities of the ligands ^{R}L are nearly zero. This suggests that the reduction occurs at the Ni center rather than β-diketiminate ligands; thus, the reduced complexes have a Ni^{I} d^9 character. This notion is also consistent with the MO analysis shown in Figure S20, Supporting Information. The $3d_{yz}$ orbital is now occupied by two electrons in the reduced complex, whereas it is singly occupied in the neutral and oxidized complexes.

TD-DFT Calculations. We used TD-B3LYP(SMD)/BS-I methods based on LC-OLYP-optimized structures to analyze UV−vis−NIR spectra of $[Ni^{II}(^{R}L^{-})_2]$, $[Ni^{II}(^{R}L^{0.5\bullet-})_2]^+$, and $[Ni^{I}(^{R}L^{-})_2]^-$.[100] The results are given in the Supporting Information. As shown in Figure S27 and Table S12, Supporting Information, the maximum absorbance of 368.8 nm with the largest oscillator strength in $[Ni^{II}(^{H}L^{-})_2]$ was assigned as MLCT and $\pi-\pi^*$ transitions. The oxidized complex $[Ni^{II}(^{H}L^{0.5\bullet-})_2]^+$ in Figure S29, Supporting Information, displays two strong signals at 361.1 and 678.0 nm assigned as $\pi-\pi^*$/LMCT and $\pi-\pi^*$ transitions, respectively. Note that in the previous studies on the oxidized L2 complex[7] the electronic transition energies of 408 and 724 nm were assigned as LMCT and MLCT, respectively, using the TD-B3LYP(COSMO)/BS-I method. More $\pi-\pi^*$ character assigned in the present system $[Ni^{II}(^{H}L^{0.5\bullet-})_2]^+$ may be attributed to the distortion from the tetrahedral geometry of the Ni^{II} center due to the *N*-phenyl substituents on the β-diketiminate ligands (DFT-predicted twist angles of 81° in the oxidized L2 complex as compared with 73° in $[Ni^{II}(^{H}L^{0.5\bullet-})_2]^+$). In addition to the two bands, a weak absorption band at 2467.6 nm of $[Ni^{II}(^{H}L^{0.5\bullet-})_2]^+$ is assigned to LLIVCT. Since the lowest occupied natural transition orbital (LUNTO) and the highest unoccupied natural transition orbital (HONTO)[101] are delocalized over β-diketiminate ligands, this oxidized complex is characterized as a class III complex. In other oxidized complexes with various

dx.doi.org/10.1021/ic5006693 | Inorg. Chem. 2014, 53, 6159−6169

substituents, LLIVCT was also observed in the NIR region. For a complex of $[Ni^{II}(^{NO2}L^{-})_2]$, the electronic absorption observed at 349 nm is assigned as a MLCT transition rather than a $\pi-\pi^*$ transition, and for the reduced complex $[Ni^{I}(^{NO2}L^{-})_2]^{-}$, absorption bands at 324 and 481 nm are assigned as MLCT/$\pi-\pi^*$ and MLCT.

SUMMARY

In this study, we synthesized a series of nickel(II) complexes with β-diketiminate ligands ($^{R}L^{-}$; R = Me, H, Br, CN, and NO_2), which exhibit a wide range of oxidation potentials. One-electron oxidation of those complexes occurs at the β-diketiminate ligands rather than at the nickel ion. Wieghardt and co-workers reported oxidation of a similar nickel complex bearing β-diketiminate ligands.[7] However, detailed characterization of the oxidation product including observation of the LLIVCT band and X-ray crystal structure have not been reported.[7] Ancillary phenyl groups of the presented complexes may enhance the stability of the one-electron-oxidized species of the complexes by intramolecular $\pi-\pi^{+\bullet}$ interactions, allowing us to determine the X-ray crystal structure of one of the cationic complexes. The centrosymmetric crystal structure and relatively sharp NIR-absorption band of the cationic complex suggested that the charge of the one-electron oxidized ligands is highly delocalized over two β-diketiminate ligands to afford a class III type oxidation state in Robin−Day classification, regardless of the difference in the one-electron oxidation potentials of starting neutral complexes extending from −0.05 V vs Fc/Fc^{+} to 0.90 V. A wide range of DFT studies also suggested the highly delocalized state of radicals produced by the oxidations. To our delight, the highly stable systems have provided excellent opportunities to examine one-electron reductions of the complexes. In contrast to the case of one-electron oxidation, one-electron reduction of the complexes mainly occurred on the nickel center to produce the nickel(I) complexes, which showed clear EPR signals due to the $S = 1/2$ species. This work has demonstrated promising potential of the β-diketiminate ligands to expand the redox ability of transition-metal complexes and bis-β-diketiminate nickel complexes as a new class of ligand-centered mixed-valence compounds.

ASSOCIATED CONTENT

Supporting Information

Crystallographic information in CIF format, Tables S1−S23, and Figures S1−S51. This material is available free of charge via the Internet at http://pubs.acs.org.

AUTHOR INFORMATION

Corresponding Authors

*E-mail: smori@mx.ibaraki.ac.jp.

*E-mail: shinobu@mls.eng.osaka-u.ac.jp.

Notes

The authors declare no competing financial interest.

ACKNOWLEDGMENTS

This work was partly supported by Grants 22105007 (to S.I.), 25105707 (to S.M.), and 24109015 (to H.S.) for Scientific Research on Innovative Areas from MEXT of Japan and by a JSPS fellowship for young scientists (Y.M.), and ALCA fund from Japan Science Technology Agency (to S.F. and K.O.). The authors express their thanks to the JSPS Japanese-German Graduate Externship Program on "Environmentally Benign Bio- and Chemical Processes" for financial support. The generous allotment of computation time from the Research Center for Computational Science (RCCS), the National Institutes of Natural Sciences, Japan, is also gratefully acknowledged.

REFERENCES

(1) Bourget-Merle, L.; Lappert, M. F.; Severn, J. R. *Chem. Rev.* **2002**, *102*, 3031−3066.
(2) Mindiola, D. J. *Acc. Chem. Res.* **2006**, *39*, 813−821.
(3) Wu, J.; Yu, T.-L.; Chen, C.-T.; Lin, C.-C. *Coord. Chem. Rev.* **2006**, *250*, 602−626.
(4) Cramer, C. J.; Tolman, W. B. *Acc. Chem. Res.* **2007**, *40*, 601−608.
(5) Holland, P. L. *Acc. Chem. Res.* **2008**, *41*, 905−914.
(6) Tsai, Y.-C. *Coord. Chem. Rev.* **2012**, *256*, 722−758.
(7) Khusniyarov, M. M.; Bill, E.; Weyhermüller, T.; Bothe, E.; Wieghardt, K. *Angew. Chem., Int. Ed.* **2011**, *50*, 1652−1655.
(8) Moilanen, J.; Borau-Garcia, J.; Roesler, R.; Tuononen, H. M. *Chem. Commun.* **2012**, *48*, 8949−8951.
(9) Radzewich, C. E.; Coles, M. P.; Jordan, R. F. *J. Am. Chem. Soc.* **1998**, *120*, 9384−9385.
(10) Fekl, U.; Kaminsky, W.; Goldberg, K. I. *J. Am. Chem. Soc.* **2001**, *123*, 6423−6424.
(11) Jazdzewski, B. A.; Holland, P. L.; Pink, M.; Young, V. G.; Spencer, D. J. E.; Tolman, W. B. *Inorg. Chem.* **2001**, *40*, 6097−6107.
(12) Yokota, S.; Tachi, Y.; Itoh, S. *Inorg. Chem.* **2002**, *41*, 1342−1344.
(13) Robin, M. B.; Day, P. In *Advances in Inorganic Chemistry and Radiochemistry*; Emeléus, H. J., Sharpe, A. G., Eds.; Academic Press: New York, 1968; Vol. *10*, pp 247−422.
(14) Hush, N. S. *Electrochim. Acta* **1968**, *13*, 1005−1023.
(15) Hush, N. S. In *Progress in Inorganic Chemistry*; John Wiley & Sons, Inc.: New York, 2007; pp 391−444.
(16) D'Alessandro, D. M.; Keene, F. R. *Chem. Soc. Rev.* **2006**, *35*, 424−440.
(17) Lynch, M. W.; Hendrickson, D. N.; Fitzgerald, B. J.; Pierpont, C. G. *J. Am. Chem. Soc.* **1984**, *106*, 2041−2049.
(18) Adams, D. M.; Hendrickson, D. N. *J. Am. Chem. Soc.* **1996**, *118*, 11515−11528.
(19) Chang, H. C.; Miyasaka, H.; Kitagawa, S. *Inorg. Chem.* **2001**, *40*, 146−156.
(20) Herebian, D.; Bothe, E.; Neese, F.; Weyhermuller, T.; Wieghardt, K. *J. Am. Chem. Soc.* **2003**, *125*, 9116−9128.
(21) Chlopek, K.; Bothe, E.; Neese, F.; Weyhermuller, T.; Wieghardt, K. *Inorg. Chem.* **2006**, *45*, 6298−6307.
(22) Ray, K.; Bill, E.; Weyhermuller, T.; Wieghardt, K. *J. Am. Chem. Soc.* **2005**, *127*, 5641−5654.
(23) Ray, K.; Weyhermuller, T.; Neese, F.; Wieghardt, K. *Inorg. Chem.* **2005**, *44*, 5345−5360.
(24) Kokatam, S.; Weyhermuller, T.; Bothe, E.; Chaudhuri, P.; Wieghardt, K. *Inorg. Chem.* **2005**, *44*, 3709−3717.
(25) Bill, E.; Bothe, E.; Chaudhuri, P.; Chlopek, K.; Herebian, D.; Kokatam, S.; Ray, K.; Weyhermuller, T.; Neese, F.; Wieghardt, K. *Chem.−Eur. J.* **2004**, *11*, 204−224.
(26) Das, D.; Sarkar, B.; Mondal, T. K.; Mobin, S. M.; Fiedler, J.; Kaim, W.; Lahiri, G. K. *Inorg. Chem.* **2011**, *50*, 7090−7098.
(27) Boyer, J. L.; Cundari, T. R.; DeYonker, N. J.; Rauchfuss, T. B.; Wilson, S. R. *Inorg. Chem.* **2009**, *48*, 638−645.
(28) Lu, C. C.; Bill, E.; Weyhermüller, T.; Bothe, E.; Wieghardt, K. *J. Am. Chem. Soc.* **2008**, *130*, 3181−3197.
(29) Lu, C. C.; Weyhermüller, T.; Bill, E.; Wieghardt, K. *Inorg. Chem.* **2009**, *48*, 6055−6064.
(30) Pratt, R. C.; Stack, T. D. P. *J. Am. Chem. Soc.* **2003**, *125*, 8716−8717.
(31) Shimazaki, Y.; Stack, T. D. P.; Storr, T. *Inorg. Chem.* **2009**, *48*, 8383−8392.

(32) Shimazaki, Y.; Tani, F.; Fukui, K.; Naruta, Y.; Yamauchi, O. *J. Am. Chem. Soc.* **2003**, *125*, 10512−10513.
(33) Shimazaki, Y.; Yajima, T.; Tani, F.; Karasawa, S.; Fukui, K.; Naruta, Y.; Yamauchi, O. *J. Am. Chem. Soc.* **2007**, *129*, 2559−2568.
(34) Rotthaus, O.; Jarjayes, O.; Perez Del Valle, C.; Philouze, C.; Thomas, F. *Chem. Commun.* **2007**, 4462−4464.
(35) Rotthaus, O.; Thomas, F.; Jarjayes, O.; Philouze, C.; Saint-Aman, E.; Pierre, J.-L. *Chem.−Eur. J.* **2006**, *12*, 6953−6962.
(36) Rotthaus, O.; Jarjayes, O.; Thomas, F.; Philouze, C.; Perez Del Valle, C.; Saint-Aman, E.; Pierre, J.-L. *Chem.−Eur. J.* **2006**, *12*, 2293−2302.
(37) Storr, T.; Verma, P.; Pratt, R. C.; Wasinger, E. C.; Shimazaki, Y.; Stack, T. D. P. *J. Am. Chem. Soc.* **2008**, *130*, 15448−15459.
(38) Storr, T.; Verma, P.; Shimazaki, Y.; Wasinger, E. C.; Stack, T. D. P. *Chem.−Eur. J.* **2010**, *16*, 8980−8983.
(39) Storr, T.; Wasinger, E. C.; Pratt, R. C.; Stack, T. D. P. *Angew. Chem., Int. Ed.* **2007**, *46*, 5198−5201.
(40) Orio, M.; Jarjayes, O.; Kanso, H.; Philouze, C.; Neese, F.; Thomas, F. *Angew. Chem., Int. Ed.* **2010**, *49*, 4989−4992.
(41) Kochem, A.; Orio, M.; Jarjayes, O.; Neese, F.; Thomas, F. *Chem. Commun.* **2010**, *46*, 6765−6767.
(42) Benisvy, L.; Kannappan, R.; Song, Y.-F.; Milikisyants, S.; Huber, M.; Mutikainen, I.; Turpeinen, U.; Gamez, P.; Bernasconi, L.; Baerends, E. J.; Hartl, F.; Reedijk, J. *Eur. J. Inorg. Chem.* **2007**, *2007*, 637−642.
(43) Pratt, R. C.; Lyons, C. T.; Wasinger, E. C.; Stack, T. D. P. *J. Am. Chem. Soc.* **2012**, *134*, 7367−7377.
(44) Kurahashi, T.; Fujii, H. *Inorg. Chem.* **2013**, *52*, 3908−3919.
(45) Dunn, T. J.; Chiang, L.; Ramogida, C. F.; Hazin, K.; Webb, M. I.; Katz, M. J.; Storr, T. *Chem.−Eur. J.* **2013**, *19*, 9606−9618.
(46) Lyons, C. T.; Stack, T. D. P. *Coord. Chem. Rev.* **2013**, *257*, 528−540.
(47) Kurahashi, T.; Fujii, H. *J. Am. Chem. Soc.* **2011**, *133*, 8307−8316.
(48) Kochem, A.; Kanso, H.; Baptiste, B.; Arora, H.; Philouze, C.; Jarjayes, O.; Vezin, H.; Luneau, D.; Orio, M.; Thomas, F. *Inorg. Chem.* **2012**, *51*, 10557−10571.
(49) de Bellefeuille, D.; Askari, M. S.; Lassalle-Kaiser, B.; Journaux, Y.; Aukauloo, A.; Orio, M.; Thomas, F.; Ottenwaelder, X. *Inorg. Chem.* **2012**, *51*, 12796−12804.
(50) Creutz, C.; Taube, H. *J. Am. Chem. Soc.* **1969**, *91*, 3988−&.
(51) Creutz, C.; Taube, H. *J. Am. Chem. Soc.* **1973**, *95*, 1086−1094.
(52) Bernhardt, P. V.; Bozoglián, F.; Macpherson, B. P.; Martínez, M. *Coord. Chem. Rev.* **2005**, *249*, 1902−1916.
(53) Sato, O.; Iyoda, T.; Fujishima, A.; Hashimoto, K. *Science* **1996**, *272*, 704−705.
(54) Ward, M. D. *Chem. Soc. Rev.* **1995**, *24*, 121−134.
(55) Soncini, A.; Mallah, T.; Chibotaru, L. F. *J. Am. Chem. Soc.* **2010**, *132*, 8106−8114.
(56) Kobayashi, A.; Kitagawa, H. *J. Am. Chem. Soc.* **2006**, *128*, 12066−12067.
(57) Armarego, W. L. F.; Chai, C. L. L. In *Purification of Laboratory Chemicals*, 6th ed.; Butterworth-Heinemann: Oxford, 2009.
(58) Klimko, V. T.; Skoldinov, A. P. *Zh. Obshch. Khim.* **1959**, *29*, 4027−4029.
(59) Tsybina, N. M.; Vinokurov, V. G.; Protopopova, T. V.; Skoldinov, A. P. *J. Gen. Chem. URRS* **1966**, *36*, 1383−1385.
(60) Shimokawa, C.; Yokota, S.; Tachi, Y.; Nishiwaki, N.; Ariga, M.; Itoh, S. *Inorg. Chem.* **2003**, *42*, 8395−8405.
(61) Todoroki, R.; Ono, M.; Tamura, S. *Heterocycles* **1986**, *24*, 755−769.
(62) Frisch, M. J.; Trucks, G. W.; Schlegel, H. B.; Scuseria, G. E.; Robb, M. A.; Cheeseman, J. R.; Scalmani, G.; Barone, V.; Mennucci, B.; Petersson, G. A.; Nakatsuji, H.; Caricato, M.; Li, X.; Hratchian, H. P.; Izmaylov, A. F.; Bloino, J.; Zheng, G.; Sonnenberg, J. L.; Hada, M.; Ehara, M.; Toyota, K.; Fukuda, R.; Hasegawa, J.; Ishida, M.; Nakajima, T.; Honda, Y.; Kitao, O.; Nakai, H.; Vreven, T.; Montgomery, J. A., Jr.; Peralta, J. E.; Ogliaro, F.; Bearpark, M.; Heyd, J. J.; Brothers, E.; Kudin, K. N.; Staroverov, V. N.; Kobayashi, R.; Normand, J.; Raghavachari, K.; Rendell, A.; Burant, J. C.; Iyengar, S. S.; Tomasi, J.; Cossi, M.; Rega, N.; Millam, J. M.; Klene, M.; Knox, J. E.; Cross, J. B.; Bakken, V.; Adamo, C.; Jaramillo, J.; Gomperts, R.; Stratmann, R. E.; Yazyev, O.; Austin, A. J.; Cammi, R.; Pomelli, C.; Ochterski, J. W.; Martin, R. L.; Morokuma, K.; Zakrzewski, V. G.; Voth, G. A.; Salvador, P.; Dannenberg, J. J.; Dapprich, S.; Daniels, A. D.; Farkas, O.; Foresman, J. B.; Ortiz, J. V.; Cioslowski, J.; Fox, D. J. *Gaussian 09*, Revision D.01; Gaussian, Inc.: Wallingford, CT, 2009.
(63) Becke, A. D. *J. Chem. Phys.* **1993**, *98*, 5648−5652.
(64) Lee, C.; Yang, W.; Parr, R. G. *Phys. Rev. B* **1988**, *37*, 785−789.
(65) Hay, P. J.; Wadt, W. R. *J. Chem. Phys.* **1985**, *82*, 270−283.
(66) Curtiss, L. A.; McGrath, M. P.; Blaudeau, J.-P.; Davis, N. E.; Binning, R. C., Jr.; Radom, L. *J. Chem. Phys.* **1995**, *103*, 6104−6413.
(67) Yanai, T.; Tew, D. P.; Handy, N. C. *Chem. Phys. Lett.* **2004**, *393*, 51−57.
(68) Tawada, Y.; Tsuneda, T.; Yanagisawa, S.; Yanai, T.; Hirao, K. *J. Chem. Phys.* **2004**, *120*, 8425−8433.
(69) Dennington, I. R.; Keith, T.; Millam, J.; Eppinnett, K.; Hovell, W. L.; Gilliland, R. *GaussView*; Semichem: Shawnee Mission, KS, 2003.
(70) Schaefer, A.; Huber, C.; Ahlrichs, R. *J. Chem. Phys.* **1994**, *100*, 5829−5835.
(71) Stratmann, R. E.; Scuseria, G. E.; Frisch, M. J. *J. Chem. Phys.* **1998**, *109*, 8218−8224.
(72) Casida, M. E. In *Recent Advances in Computational Chemistry*; Chong, D. P., Ed.; World Scientific: New York, 1995; Vol. *1*, pp 155−192.
(73) NBO Version 5.G implemented by Glendening, E. D.; Reed, A. E.; Carpenter J. E.; Weinhold, F., 2005.
(74) Barone, V.; Cossi, M. *J. Phys. Chem. A* **1998**, *102*, 1995−2001.
(75) Marenich, A. V.; Cramer, C. J.; Truhlar, D. G. *J. Phys. Chem. B* **2009**, *113*, 6378−6396.
(76) Healy, P.; Bendall, M.; Doddrell, D.; Skelton, B.; White, A. *Aust. J. Chem.* **1979**, *32*, 727−735.
(77) Parks, J. E.; Holm, R. H. *Inorg. Chem.* **1968**, *7*, 1408−1416.
(78) Song, L.; Trogler, W. C. *Angew. Chem., Int. Ed.* **1992**, *31*, 770−772.
(79) Ghosh, P. K.; Brunschwig, B. S.; Chou, M.; Creutz, C.; Sutin, N. *J. Am. Chem. Soc.* **1984**, *106*, 4772−4783.
(80) Nelsen, S. F. *Chem.−Eur. J.* **2000**, *6*, 581−588.
(81) Demadis, K. D.; Hartshorn, C. M.; Meyer, T. J. *Chem. Rev.* **2001**, *101*, 2655−2685.
(82) Brunschwig, B. S.; Creutz, C.; Sutin, N. *Chem. Soc. Rev.* **2002**, *31*, 168−184.
(83) McManis, G. E.; Nielson, R. M.; Weaver, M. J. *Inorg. Chem.* **1988**, *27*, 1827−1829.
(84) Lambert, C.; Nöll, G. *Angew. Chem., Int. Ed.* **1998**, *37*, 2107−2110.
(85) Shimazaki, Y.; Arai, N.; Dunn, T. J.; Yajima, T.; Tani, F.; Ramogida, C. F.; Storr, T. *Dalton Trans.* **2011**, *40*, 2469−2479.
(86) Takai, A.; Yasuda, T.; Ishizuka, T.; Kojima, T.; Takeuchi, M. *Angew. Chem., Int. Ed.* **2013**, *52*, 9167−9171.
(87) Small, D.; Zaitsev, V.; Jung, Y.; Rosokha, S. V.; Head-Gordon, M.; Kochi, J. K. *J. Am. Chem. Soc.* **2004**, *126*, 13850−13858.
(88) Sun, D. L.; Rosokha, S. V.; Lindeman, S. V.; Kochi, J. K. *J. Am. Chem. Soc.* **2003**, *125*, 15950−15963.
(89) Li, M.; Neal, T. J.; Wyllie, G. R. A.; Oliver, A. G.; Schulz, C. E.; Scheidt, W. R. *Inorg. Chem.* **2011**, *50*, 9114−9121.
(90) Herwig, P. T.; Enkelmann, V.; Schmelz, O.; Müllen, K. *Chem.−Eur. J.* **2000**, *6*, 1834−1839.
(91) Gennett, T.; Milner, D. F.; Weaver, M. J. *J. Phys. Chem.* **1985**, *89*, 2787−2794.
(92) Holland, P. L.; Cundari, T. R.; Perez, L. L.; Eckert, N. A.; Lachicotte, R. J. *J. Am. Chem. Soc.* **2002**, *124*, 14416−14424.
(93) Bai, G.; Wei, P.; Stephan, D. W. *Organometallics* **2005**, *24*, 5901−5908.
(94) Pfirrmann, S.; Limberg, C.; Herwig, C.; Stößer, R.; Ziemer, B. *Angew. Chem., Int. Ed.* **2009**, *48*, 3357−3361.
(95) Xiong, Y.; Yao, S.; Bill, E.; Driess, M. *Inorg. Chem.* **2009**, *48*, 7522−7524.

(96) Pfirrmann, S.; Yao, S.; Ziemer, B.; Stösser, R.; Driess, M.; Limberg, C. *Organometallics* **2009**, *28*, 6855−6860.
(97) Pfirrmann, S.; Limberg, C.; Herwig, C.; Knispel, C.; Braun, B.; Bill, E.; Stösser, R. *J. Am. Chem. Soc.* **2010**, *132*, 13684−13691.
(98) Singh, A. P.; Samuel, P. P.; Roesky, H. W.; Schwarzer, M. C.; Frenking, G.; Sidhu, N. S.; Dittrich, N. *J. Am. Chem. Soc.* **2013**, *135*, 7324−7329.
(99) Tim Storr, E. C. W.; Pratt, Russell C.; Daniel, T.; Stack, P. *Angew. Chem., Int. Ed.* **2007**, *46*, 5198−5201.
(100) Diffuse functions were added for C, N, and Ni atoms into the def2SVP basis sets (denoted as def2SVP(+)) in $[Ni^{I}(^{H}L^{-})_2]^{-}$ and $[Ni^{I}(^{CN}L^{-})_2]^{-}$ for geometry optimizations and TD-DFT calculations. The RMSDs (for heavy atoms) of 0.044 and 0.071 Å for $[Ni^{I}(^{H}L^{-})_2]^{-}$ and $[Ni^{I}(^{CN}L^{-})_2]^{-}$ are found to be very small.
(101) Jakubikova, E.; Chen, W.; Dattelbaum, D. M.; Rein, F. N.; Rocha, R. C.; Martin, R. L.; Batista, E. R. *Inorg. Chem.* **2009**, *48*, 10720−10725.

dx.doi.org/10.1021/ic5006693 | *Inorg. Chem.* 2014, 53, 6159−6169